

Peter C. Tandy

DSE Perspective on QCD Modeling, Distribution Amplitudes, and Form Factors

April 2, 2014

PACS 12.38.Aw, 12.38.Lg, 14.40.Be, 13.40.Gp

Abstract We describe results for the pion distribution amplitude (PDA) at the non-perturbative scale $\mu = 2$ GeV by projecting the Poincaré-covariant Bethe-Salpeter wave-function onto the light-front and use it to investigate the ultraviolet behavior of the electromagnetic form factor, $F_\pi(Q^2)$, on the entire domain of spacelike Q^2 . The significant dilation of this PDA compared to the known asymptotic PDA is a signature of dynamical chiral symmetry breaking (DCSB) on the light front. We investigate the transition region of Q^2 where non-perturbative behavior of constituent-like quarks gives way to the partonic-like behavior of quantum chromodynamics (QCD). The non-perturbative approach is based on the Dyson-Schwinger equation (DSE) framework for continuum investigations in QCD. The leading-order, leading-twist perturbative QCD result for $Q^2 F_\pi(Q^2)$ underestimates the new DSE computation by just 15% on $Q^2 \gtrsim 8 \text{ GeV}^2$, in stark contrast with the result obtained using the asymptotic PDA.

Keywords Non-perturbative continuum modeling of QCD · Pion distribution amplitude · Asymptotic QCD · Pion charge form factor · Dyson-Schwinger approach · Dynamical chiral symmetry breaking

1 Introduction

A light front formulation of QCD can translate features that arise purely through the infinitely-many-body nature of relativistic quantum field theory into images whose interpretation is similar to quantum mechanical probability amplitudes. A phenomenon for which a quantum mechanical image would be desirable is dynamical chiral symmetry breaking (DCSB). Strictly impossible in quantum mechanics with a finite number of degrees-of-freedom, this emergent feature of QCD correlates numerous aspects of the spectrum and interactions of hadrons; e.g., the large splitting between parity partners [1; 2] and the existence and location of a zero in some hadron form factors [3]. However DCSB has not yet been realized in the light-front formulation of quantum field theory.

The impact of DCSB is expressed with particular force in properties of the pion—the pseudo-Goldstone boson. Its very existence as the lightest hadron is grounded in DCSB. The modern paradigm views the pion as both a conventional bound-state in quantum field theory and the Goldstone mode associated with DCSB in QCD. Numerous model-independent statements may be made about the pion’s Bethe-Salpeter amplitude and its relationship to the dressed-quark propagator [4]. We review here the recent extraction of the pion’s light-front valence-quark distribution amplitude (PDA) computed from these two quantities. The results expose DCSB in a covariant wave-function projected onto the light front.

Work supported in part by National Science Foundation Grant No. NSF-PHY-1206187

P. Tandy

Department of Physics, Kent State University, Kent, Ohio, 44242 USA

E-mail: tandy@kent.edu

There exist exact results and empirically satisfactory results for both soft and hard scattering processes as described in recent reviews [5; 6; 7]. While the comparison between low-energy experiments and theory check global symmetries and breaking patterns that can be characteristic of a broad class of theories, the high-energy experiments and calculations are a direct probe of specific details of QCD itself; and there are unresolved issues. Resolutions for a couple of these are discussed here.

2 Pion Distribution Amplitude

The leading twist 2-particle PDA is given by¹

$$f_\pi \varphi_\pi(x; \mu) = Z_2 \text{tr}_{\text{CD}} \int_{dk}^\Lambda \delta(n \cdot k - x n \cdot P) \gamma_5 \gamma \cdot n \chi_\pi(k; P), \quad (1)$$

where: f_π is the pion's leptonic decay constant; the trace is over color and spinor indices; \int_{dk}^Λ is a Poincaré-invariant regularization of the four-dimensional integral, with Λ the ultraviolet regularization mass-scale; $Z_2(\mu, \Lambda)$ is the quark wave-function renormalisation constant, with μ the renormalisation scale; n is a light-like four-vector, $n^2 = 0$; P is the pion's four-momentum, $P^2 = -m_\pi^2$ and $n \cdot P = -m_\pi$, with m_π being the pion's mass; and the pion's Bethe-Salpeter wave-function is $\chi_\pi(k; P) = S(k) \Gamma_\pi(q; P) S(k - P)$ with Γ_π the Bethe-Salpeter amplitude, S the dressed light-quark propagator, and $q = k - P/2$ is a convenient relative momentum variable for expression of symmetries. As a framework within continuum quantum field theory, the DSE study of Ref. [8] was able to reliably compute arbitrarily many moments $\langle x^m \rangle := \int_0^1 dx x^m \varphi_\pi(x)$ of the PDA which Eq. (1) yields in the form

$$\langle x^m \rangle = \frac{N_c Z_2}{f_\pi (n \cdot P)^{m+1}} \text{tr}_D \int_{dk}^\Lambda (n \cdot k)^m \gamma_5 \gamma \cdot n \chi_\pi(k; P). \quad (2)$$

The dressed-quark propagator, having the general form $S(p) = 1/[i\gamma \cdot p A(p^2, \mu^2) + B(p^2, \mu^2)]$, can be obtained from the relevant DSE, namely the gap equation [5; 6]:

$$S^{-1}(p) = Z_2 (i\gamma \cdot p + m^{\text{bm}}) + Z_1 \int_{dq}^\Lambda g^2 D_{\mu\nu}(p - q) \frac{\lambda^a}{2} \gamma_\mu S(q) \frac{\lambda^a}{2} \Gamma_\nu(q, p), \quad (3)$$

where: $D_{\mu\nu}$ is the dressed gluon propagator; Γ_ν the quark-gluon vertex; $m^{\text{bm}}(\Lambda)$ the current-quark bare mass; and $Z_1(\mu, \Lambda)$ the vertex renormalization constant. We employ the renormalisation procedures of Ref. [9] except that the present work uses the renormalization point, $\mu = 2 \text{ GeV}$ to facilitate comparison with existing lattice-QCD information on a few moments of $\varphi_\pi(x; \mu)$. Numerous features of the gap equation, its kernel, and the solution procedure are described in Ref. [9]. The amplitude Γ_π may be obtained from the Bethe-Salpeter equation, a modern expression of which is explained in Ref. [10]. The general form is

$$\Gamma_\pi(q; P) = \gamma_5 [iE_\pi(q; P) + \gamma \cdot P F_\pi(q; P) + q \cdot P \gamma \cdot q G_\pi(q; P) + \sigma_{\mu\nu} q_\mu P_\nu H_\pi(q; P)], \quad (4)$$

where the functions are even in $q \cdot P$. In the chiral limit, $m_\pi = 0$ giving the Goldberger-Treiman-like identity $f_\pi E_\pi(q; 0) = B(q^2)$. This is a pointwise statement of Goldstone's theorem and part of a near complete equivalence between the one-quark problem and the ground state pseudoscalar two-body problem in QCD. The gap and Bethe-Salpeter equations are key members of the set of Dyson-Schwinger equations (DSEs), which provide an efficacious tool for the study of hadron properties [5; 6; 7].

In Ref. [8], 50 moments were produced from Eq. (2) by employing the interaction of Ref. [13] under two different procedures: rainbow-ladder truncation (RL), a very widely used DSE computational scheme in hadron physics, detailed in App. A.1 of Ref. [14]; and the DCSB-improved kernel (DB) [10] detailed in App. A.2 of Ref. [14]. Both schemes are symmetry-preserving, and produce DCSB and Goldstone's theorem, but the DB procedure incorporates nonperturbative effects associated with DCSB into the kernel itself, and is thus more realistic. The DB kernel thereby exposes a key role played by the dressed-quark anomalous chromomagnetic moment in determining observable quantities [15; 1]. The

¹ We use a Euclidean metric: $\{\gamma_\mu, \gamma_\nu\} = 2\delta_{\mu\nu}$; $\gamma_\mu^\dagger = \gamma_\mu$; $\gamma_5 = \gamma_4 \gamma_1 \gamma_2 \gamma_3$, $\text{tr}[\gamma_5 \gamma_\mu \gamma_\nu \gamma_\rho \gamma_\sigma] = -4\epsilon_{\mu\nu\rho\sigma}$; $\sigma_{\mu\nu} = (i/2)[\gamma_\mu, \gamma_\nu]$; $a \cdot b = \sum_{i=1}^4 a_i b_i$; and P_μ timelike $\Rightarrow P^2 < 0$.

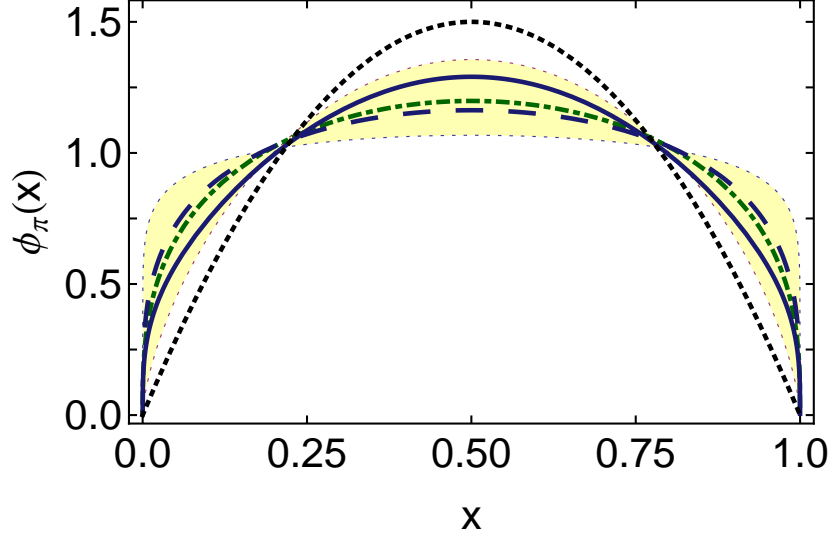


Fig. 1 $\phi_\pi(x; \mu)$ at $\mu = 2$ GeV. Dot-dashed curve, as determined [11] from a single lattice-QCD moment [12] by fitting α according to Eq. (9). The shaded region reflects the associated uncertainty. The DSE results [8] described in the text are also depicted: solid curve, the DSE-DB result; dashed curve, the DSE-RL result. The dotted curve is $\phi_\pi^{\text{asy}}(x)$.

renormalization scale $\mu = 2$ GeV is used to enable direct comparison with lattice-QCD results. The kernel strength is specified by a product: $D\omega = m_G^3$, and the effective gluon mass $m_G = 0.87$ GeV is the only relevant parameter fitted to properties of ground-state vector and flavor-nonsinglet pseudoscalar mesons [13].

The calculation of Eq. (2) employed generalized Nakanishi representations [16; 17; 18] for $S(p)$ and $\Gamma_\pi(k; P)$ that are found to provide excellent parameterizations of previous numerical solutions for $S(k)$ and $\Gamma_\pi(q; P)$ [13; 8]. The employed representation for the dressed quark propagator is [19]

$$S(p) = \sum_{j=1}^{n_p} \left(\frac{z_j}{i\not{p} + m_j} + \frac{z_j^*}{i\not{p} + m_j^*} \right), \quad (5)$$

where $n_p = 2$ pairs of complex conjugate mass poles is found to be sufficient here. The Nakanishi-type representation of the pion's Bethe-Salpeter invariant amplitudes \mathcal{F}_σ , with $\sigma = E, F, G, H$, can be expressed as

$$\mathcal{F}_\sigma(q; P) = \int_{-1}^1 d\alpha \int_0^\infty d\beta \sum_{\gamma} \frac{\hat{\rho}_\gamma(\alpha, \beta)}{(q^2 + \alpha q \cdot P + \beta_0 + \beta)^{n_\gamma}}, \quad (6)$$

where the n_γ are integers, and $\beta_0 > 0$. It is found that with $n_t = 3$ and $\hat{\rho}_\gamma(\alpha, \beta) = \rho_\gamma(\alpha) \delta(\beta + \beta_0 - \Lambda_\gamma^2)$ an excellent representation of numerical solutions is obtained. For further details and the parameters of Eq. (5) and Eq. (6) see Ref. [8]. With these representations the quark loop integral Eq. (2) becomes

$$\langle x^m \rangle \propto \sum_{\sigma} \int_{-1}^1 d\alpha \rho_\gamma(\alpha) I_\sigma^m(\alpha, n, P), \quad (7)$$

where $\sigma = \gamma, j_1, j_2$ denotes the set of discrete summation labels for the bound state vertex and the two propagators,

$$I_\sigma^m(\alpha, n, P) = \int \frac{d^4 k}{(2\pi)^4} \frac{N_\sigma^m(k, n, P)}{\mathcal{D}_\sigma(k, P; \alpha)}, \quad (8)$$

and $\mathcal{D}_\sigma = [D_\gamma(k, P; \alpha)]^{n_\gamma} D_{j_1}(k, P) D_{j_2}(k) R(k)$. With $R(k) = (1 + k^2/\Lambda^2)$ being the ultraviolet regulator, each denominator factor of the integrand for I_σ^m is a quadratic form in k and the numerator N_σ^m

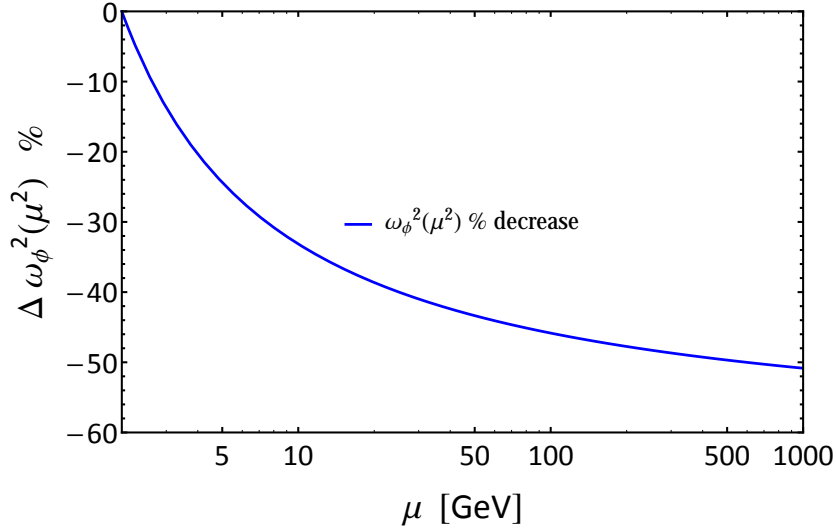


Fig. 2 The % change in $\omega_\phi^2(\mu)$ relative to its value at $\mu = 2$ GeV as it is evolved to higher scales.

contains only limited finite powers, and both are Lorentz invariant. Use of the standard techniques associated with the Feynman integrals familiar from perturbation theory then yields the final result in algebraic form.

The dressed nature of propagators and vertices induces a departure from power law behavior in the ultraviolet due to the one-loop renormalization group behavior of QCD as produced by the particular DSE truncation employed. For the Nakanishi-type representations this requires incorporation of an additional ultraviolet momentum dependence like $\ln^{-\gamma_F}[p^2/\Lambda_{\text{QCD}}^2]$, where γ_F is the anomalous dimension of object F in the loop integral. A fractional power approximation to the logarithm is found to be quite accurate for the ultraviolet behavior [28]; the algebraic results for the relevant Feynman integrals are straightforward.

This technique [8] greatly simplifies the practical problem of continuing from Euclidean to Minkowski metric; it allows the use of Euclidean DSE modeling of QCD to address quantities that are naturally defined by light-front momenta. Accumulated experience in Euclidean QCD-modeling has found that, with the momentum dependence of the gap and Bethe-Salpeter equation solutions represented only by numerical arrays, the variable mass scales $\gg \Lambda_{\text{QCD}}$ encountered in treatments of hadronic observables requires a near impossible accounting for singularities in the complex p^2 plane of integration. The above method will only produce singularities in the Feynman integral result of a given process amplitude if there are observable production channels and thresholds open to that process.

2.1 Representations and comparison with lattice-QCD

From Eq. (2) the PDA moments $\{\langle x^m \rangle | m = 1, \dots, m_{\text{max}}\}$ with $m_{\text{max}} = 50$ are used to reconstruct $\phi_\pi(x; \mu)$. Since the Gegenbauer polynomials $C_n^{(\alpha+1/2)}(2x-1)$ are a complete orthonormal set on $x \in [0, 1]$ with respect to the measure $[x(1-x)]^\alpha$, they facilitate reconstruction of any function that vanishes at $x = 0, 1$ and is symmetric about $x = 1/2$. One therefore fits the $\langle x^m \rangle$ to the moments of

$$\varphi_\pi(x; \mu) = N_\alpha [x(1-x)]^\alpha \left[1 + \sum_{n=2,4,\dots}^{n_{\text{max}}} a_n^\alpha(\mu) C_n^{(\alpha+1/2)}(2x-1) \right], \quad (9)$$

where $N_\alpha = \Gamma(2\alpha+2)/[\Gamma(\alpha+1)]^2$. The value of α can be optimized to minimize the number of terms (n_{max}) needed to fit the $\langle x^m \rangle$, thus producing a rapidly convergent series. A value $n_{\text{max}} = 2$ is then found to ensure that the $\langle x^m \rangle$ are reproduced to within an RMS error of 1%. In general, the quantities α , and n_{max} are also dependent on the scale μ . The dashed curve in Fig. 1 is the RL result for the PDA

at 2 GeV. It is described by Eq. (9) with $\alpha_{\text{RL}} = 0.29$, and the only coefficient needed is $a_2^{\text{RL}} = 0.0029$. The solid curve in Fig. 1 is the DB result and it is described by Eq. (9) with $\alpha_{\text{DB}} = 0.31$, and the only coefficient needed is $a_2^{\text{DB}} = -0.12$. Compared to the asymptotic QCD result $\phi_\pi^{\text{asy}} = 6x(1-x)$, the non-perturbative PDA in Fig. 1 is significantly dilated. This can be traced to DCSB and is a long-sought and unambiguous expression of that phenomenon on the light-front [20; 21; 22].

If one were to instead impose $\alpha = 1$, then the representation in Eq. (9) becomes identical to the familiar perturbative QCD representation in terms of the Gegenbauer $C_n^{(3/2)}(2x-1)$ polynomials which are the irreducible representations of the collinear conformal group $\text{SL}(2; \mathbb{R})$ that expresses the invariance of QCD at asymptotically large scales [23; 24; 25; 26]. The scale evolution of the coefficients $a_n^{3/2}(\mu)$ is known [23; 24] and is especially simple at leading order. Because of the certainty of asymptotic QCD results, and the absence of information on $\varphi_\pi(x; \mu)$ at a non-perturbative μ , it has been common to seek a determination of the first few coefficients $a_n^{3/2}(\mu)$ with limited information from lattice-QCD, high energy exclusive scattering or the QCD sum rule approach, even though the scale would be finite [27; 12]. However, the PDA extracted from the DSE work at $\mu = 2$ GeV, when projected onto a $\{C_n^{(3/2)}\}$ -basis, shows that many more than a few coefficients $\{a_n^{3/2}\}$ are needed. For both DSE results, one needs $n_{\text{max}} > 14$ before $a_n^{3/2} < 0.1 a_2^{3/2}$ and the PDA is adequately reproduced. A truncation to $n_{\text{max}} = 4$ introduces spurious oscillations, or multiple-humped PDAs, that are typical of non-converged Fourier-like representations. Since the pion multiplet contains a charge-conjugation eigenstate, each of the three significant invariant amplitudes of $\Gamma_\pi(q; P)$ peaks at zero relative momentum q^2 and monotonically decrease with q^2 , as confirmed by solution of the Bethe-Salpeter equation. As a consequence $\varphi_\pi(x; \mu)$ should exhibit a single maximum at $x = 1/2$. In seeking to extract $\varphi_\pi(x)$ from limited information, it is better to fit α first than to force $\alpha = 1$ and infer a value for a few of the many sizable $a_n^{(3/2)}$.

That non-perturbative scales entail large corrections to $\varphi_\pi^{\text{asy}}(x)$ is illustrated by the scale evolution of the $a_n^{3/2}(\mu)$ obtained by projection of the DSE PDA. After evolution to $\mu = 100$ GeV, $a_2^{3/2}(\mu)$ has fallen to only 50% of its 2 GeV value, while $a_4^{3/2}(\mu)$ has fallen to only 37% of its 2 GeV value. These observations suggest that asymptotic QCD is quite remote from present experimental capabilities.

The PDA moment result $\langle (2x-1)^2 \rangle_{\phi_\pi} = 0.27 \pm 0.04$ was obtained from lattice-QCD [12]. With the conventional Gegenbauer-(3/2) version of Eq. (9) used to determine the single coefficient $a_2^{3/2}(\mu_2)$, a “double-humped” PDA was produced [12]. If instead one views α in Eq. (9) as the single parameter to be determined, the result is $\alpha = 0.35^{+0.32}_{-0.24}$ [11]. This compares favorably with the values 0.31 and 0.29 obtained from the two DSE kernels [8], and again indicates that very few expansion coefficients a_n^α would be needed to improve the PDA. The PDA determined this way from lattice-QCD is depicted in Fig. 1 along with the band reflecting lattice uncertainties. It produces a concave amplitude in agreement with contemporary DSE studies and confirms that $\varphi_\pi^{\text{asy}}(x)$ is not a good approximation at $\mu = 2$ GeV, and an expansion that starts with it will have poor convergence properties. Projection of this DSE-inspired fit onto the Gegenbauer-(3/2) basis allows the scale to be evolved for application to a given process. One finds that only for $\mu \gtrsim 100$ GeV is $a_2^{3/2} \lesssim 10\%$ and $a_4^{3/2}/a_2^{3/2} \lesssim 30\%$. Evidently, the influence of DCSB, which causes the PDA to be broader than the asymptotic QCD result, persists to remarkably high scales.

3 Pion Charge Form Factor

The QCD prediction for exclusive scattering at large Q^2 follows from observations that the process amplitude factorizes into a perturbative scattering amplitude that supports the flow of hard momentum convoluted with a soft amplitude carrying the non-perturbative dynamics of the initial and final hadron state [33; 23; 24]. With light front coordinates being an efficient way to represent this, hadronic distribution amplitudes enter into the description. The ultraviolet behavior of $F_\pi(Q^2)$ is of great contemporary interest. The rainbow-ladder DSE prediction [29] in 2000 for $Q^2 F_\pi(Q^2)$ in Fig. 4 agrees with the existing accurate data but it only hints at a maximum at $Q^2 \approx 6 \text{ GeV}^2$. The domain upon which this quantity flattens is expected to be accessible to next-generation experiments [31]. The QCD prediction for the pion charge form factor at suitably large Q^2 [33; 23; 24] is

$$Q^2 \gg \Lambda_{\text{QCD}}^2 : Q^2 F_\pi(Q^2) \rightarrow 16\pi\alpha_s(Q^2) f_\pi^2 \omega_\phi^2(Q^2) + \mathcal{O}(1/Q^2), \quad (10)$$

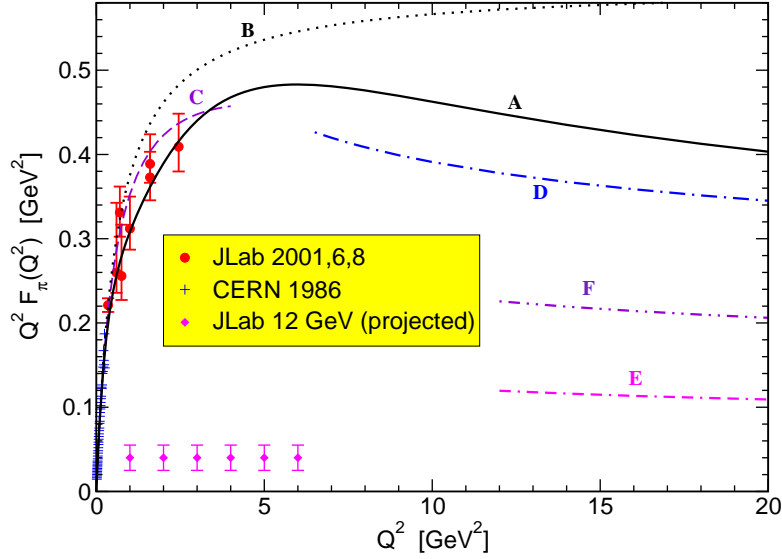


Fig. 3 $Q^2 F_\pi(Q^2)$. Solid black curve (A): the 2013 DSE result [28]; dotted black curve (B): the vector meson dominance Ansatz using the ρ mass; long dashed purple curve (C): the previous 2000 DSE result [29] that could not address $Q^2 > 4 \text{ GeV}^2$; dash-dot blue curve (D): the uv-QCD result of Eq. (10) using $\varphi_\pi(x; \mu)$ at 2 GeV; dash-dash-dot magenta curve (E): the asymptotic or conformal QCD result using $\varphi_\pi^{\text{asy}}(x)$; dash-dot-dot purple curve (F): the uv-QCD result using $\varphi_\pi(x; \mu)$ at 10 GeV. The filled red circles are the data described in Ref. [30]; and the filled diamonds indicate the projected reach and accuracy of a forthcoming experiment [31]. The short horizontal lines at very low Q^2 depict the data from Ref. [32].

where $f_\pi = 92.2 \text{ MeV}$ is the pion decay constant, and

$$\omega_\phi(\mu^2) = \frac{1}{3} \int_0^1 dx \frac{1}{x} \varphi_\pi(x; \mu). \quad (11)$$

For the purposes of Eq. (10) the choice $\mu = Q$ is representative. If one uses the asymptotic PDA $\varphi_\pi(x; \infty) = \varphi_\pi^{\text{asy}}(x)$ then $\omega_\phi \rightarrow 1$, and Eq. (10) reduces to the well-used asymptotic expression for $Q^2 F_\pi(Q^2)$ [33; 23; 24]. Just how large Q^2 must be for it to be accurate has not been clear.

At $Q^2 = 4 \text{ GeV}^2$, approximately the midpoint of the domain accessible at next-generation facilities, the asymptotic expression yields $Q^2 F_\pi(Q^2 = 4) = 0.15$ with $n_f = 4$ and $\Lambda_{\text{QCD}} = 0.234 \text{ GeV}$ [13]. This is a factor of 2.7 smaller than the empirical value ($0.41^{+0.04}_{-0.03}$) quoted at $Q^2 = 2.45 \text{ GeV}^2$ [34; 30], and a factor of three smaller than the previous DSE theory result at $Q^2 = 4 \text{ GeV}^2$ in Ref. [29]. Notably, Ref. [29] provided the only prediction for the pointwise behavior of $F_\pi(Q^2)$ that is applicable on the entire spacelike domain currently mapped reliably by experiment. It seemed a reasonable assumption that, by about $Q^2 \gtrsim 10 \text{ GeV}^2$ perturbative scattering mechanisms and partonic behavior should have set in, so that after removal of the valence quark counting power, only the slow logarithms of QCD remain. It was therefore difficult to imagine that the magnitude of $Q^2 F_\pi(Q^2)$ will fall by a factor of 3 as Q^2 covered the range 4 to 10 GeV^2 .

Two recent developments have cleared up much of this matter. Firstly, the recent DSE calculation [8] of $\varphi_\pi(x; \mu)$ provides information about $\omega_\phi(\mu^2)$ for Eq. (10) in this Q^2 range. Secondly, the DSE approach to $F_\pi(Q^2)$ has been reformulated with new methods that enable a calculation [28] to arbitrarily large- Q^2 , thus allowing a consistent examination of the transition between non-perturbative and perturbative QCD regimes. It is the quantity $\omega_\phi^2(Q^2)$ that describes how the perturbative QCD domain links to the asymptotic domain. The DSE results for $\omega_\phi(\mu^2)$ can be analyzed in terms of the equivalent number of $C_n^{(3/2)}(2x-1)$ polynomials needed if that representation is chosen for a range of μ in the ultraviolet. To reproduce more than 90% of $\omega_\phi^2(\mu)$, the number needed is 9 at $\mu = 2 \text{ GeV}$, 7 at $\mu = 4 \text{ GeV}$, and 5 at $\mu = 10 \text{ GeV}$. It is therefore necessary to build $\omega_\phi^2(\mu^2)$ from a successful description of pion structure

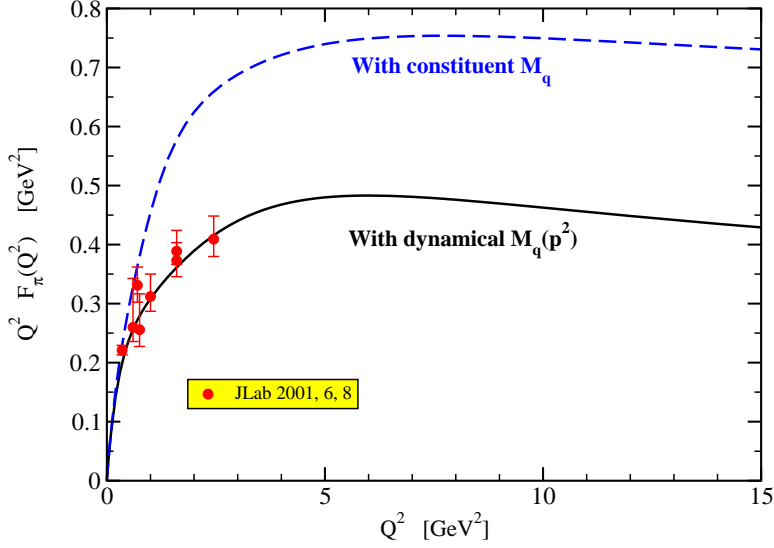


Fig. 4 Dynamical mass effect. Solid curve (black): the 2013 DSE result [28] containing the momentum-dependent quark mass dressing; dashed curve (blue): the quark propagators external to the bound state vertices are replaced by constituent mass propagators. The dynamical mass yields a reduction of about 64% near the turnover.

at non-perturbative scales. The scale evolution of the projected coefficients $a_n^{3/2}(\mu)$, and thus $\omega_\phi^2(\mu^2)$, away from the non-perturbative region is very slow. In Fig. 2 is displayed the % decrease of $\omega_\phi^2(\mu^2)$ with increasing scale, relative to its value at $\mu = 2$ GeV. Even at 1 TeV it still holds about 50% of its value associated with the non-perturbative domain.

3.1 Pion Form Factor Calculation

At leading order in the symmetry-preserving rainbow-ladder DSE truncation scheme reviewed in Refs. [5; 6], the pion form factor is given by

$$2 K_\mu F_\pi(Q^2) = N_c \text{tr}_D \int \frac{d^4 k}{(2\pi)^4} \chi_\mu(k + p_f, k + p_i) \Gamma_\pi(k_i; p_i) S(k) \Gamma_\pi(k_f; -p_f), \quad (12)$$

where Q is the incoming photon momentum, $p_{f,i} = K \pm Q/2$, $k_{f,i} = k + p_{f,i}/2$, and the remaining trace is over spinor indices. The unamputated dressed-quark-photon vertex, $\chi_\mu(k_f, k_i)$, should also be computed in RL truncation. The impact of corrections to this truncation is understood and the dominant effect is a modified power associated with the logarithmic running; in either case the running is so slow that the omitted diagrams have no material impact here.

In the most recent work [28], we employ the RL interaction of Ref. [13] and the generalized Nakanishi spectral representations [16; 17; 18] for $S(p)$ and $\Gamma_\pi(k; P)$ as described in association with Eqs. (5) and (6). In a straightforward generalization of the analysis presented earlier for the pion distribution amplitude in Eqs. (7) and (8), the calculation of $F_\pi(Q^2)$ reduces to a sum of standard Feynman integrals, and the result is an algebraic expression. For the unamputated dressed-quark-photon vertex, $\chi_\mu(k_f, k_i)$, we use an *Ansatz* with the following properties. It satisfies the longitudinal Ward-Green-Takahashi identity, is free of kinematic singularities, reduces to the bare vertex in the free-field limit, and has the same Poincaré transformation properties as the bare vertex. The *Ansatz* also includes a dressed-quark anomalous magnetic moment, made mandatory by DCSB [15]. This and other non-perturbative

corrections to the bare vertex, including the tail of the ρ -meson resonance, are negligible for spacelike momenta $Q^2 \gtrsim 1 \text{ GeV}^2$ [35; 36].

The new DSE calculation [28] of $F_\pi(Q^2)$ is displayed in Fig. 3. The dash-dash-dot curve is the prediction of QCD at a truly asymptotic scale, and uses $\varphi_\pi^{\text{asy}}(x)$. It is often characterized as the prediction of pQCD and thus relevant to the range $Q^2 \gtrsim 6 \text{ GeV}^2$ in such plots. However as discussed earlier $\varphi_\pi(x; \mu)$ is significantly broader than $\varphi_\pi^{\text{asy}}(x)$ at the displayed scales, and this makes $\omega_\phi(\mu^2)$ almost a factor of 3 larger than its asymptotic value 1.0. To be more specific, with $\varphi_\pi(x; \mu)$ taken at $\mu = 2 \text{ GeV}$, the uv-QCD prediction from Eq. (10) is shown by the dash-dot curve; this is only 15% below the most recent DSE calculation which is the solid curve [28]. With $\varphi_\pi(x; \mu)$ taken at $\mu = 10 \text{ GeV}$, the uv-QCD prediction is depicted by the dash-dot-dot curve, which is really only relevant at $Q^2 = 100 \text{ GeV}^2$ but shown here to indicate how slow is the approach to the asymptotic result². The findings can be summarized by $\omega_\phi^2(4 \text{ GeV}^2) = 3.2$, and $\omega_\phi^2(100 \text{ GeV}^2) = 2.0$, with its evolution over a wide range of scales shown in Fig. 2. Even at 1 TeV it still holds about 50% of its value associated with scales accessible to experiment.

In Fig. 4 we display the strong reduction effect that the dynamical dressing of the quark mass function has on the ultraviolet magnitude of $Q^2 F_\pi(Q^2)$. The dashed curve is the result obtained if the quark propagators evident in the triangle diagram are replaced by constituent mass propagators. The full calculation, shown by the solid curve, naturally includes the momentum-dependent evolution of the quark mass from a typical constituent value at quark momenta $k^2 \lesssim 1 \text{ GeV}^2$ to its small partonic value for $k^2 \gtrsim 4 \text{ GeV}^2$. With $k^2 \sim 2 \text{ GeV}^2$ taken as a measure of the transition region, and noting that as Q^2 increases there is a fixed spacelike bias of $Q/2$ in each quark propagator, one estimates that $Q^2 \sim 8 \text{ GeV}^2$ is a good measure of the IR-UV transition or turnover region [37]. There the dynamical mass yields a reduction of about 64%.

4 Summary

$\varphi_\pi^{\text{asy}}(x)$ is a poor approximation to $\varphi_\pi(x; \mu)$ at all momentum-transfer scales that are either now accessible to experiments involving pion elastic or transition processes, or will become so in the foreseeable future [38; 39]. Predictions of leading-order, leading-twist formulae involving $\varphi_\pi^{\text{asy}}(x)$ are a misleading guide to interpreting and understanding contemporary experiments. At accessible energy scales a better guide is obtained by using the broad PDA described herein in such formulae. This might be adequate for the charged pion's elastic form factor. However, it will probably be necessary to consider higher twist and higher-order corrections in controversial cases such as the $\gamma^* \gamma \rightarrow \pi^0$ transition form factor [40; 41; 42].

The near agreement for $Q^2 > 6 \text{ GeV}^2$ in Fig. 3 between the perturbative QCD prediction that uses $\varphi_\pi(x; 2 \text{ GeV})$ (dash-dot curve) and the new DSE result for $Q^2 F_\pi(Q^2)$ (solid curve) is striking. It highlights that a single DSE interaction kernel, essentially determined by one strength parameter, and preserving the one-loop renormalization group behavior of QCD, is very close to unifying the pion's electromagnetic form factor and its valence-quark distribution amplitude. Numerous other quantities are also correlated quite closely via a single DSE interaction kernel [5; 6; 7; 43].

Moreover, this leading-order, leading-twist QCD prediction, obtained with a pion valence-quark PDA evaluated at a scale appropriate to the experiment, underestimates our full computation by merely an approximately uniform 15% on the domain depicted. The small mismatch should be explained by a combination of higher-order, higher-twist corrections to Eq. (10) and shortcomings in the rainbow-ladder truncation, which predicts the correct power-law behavior for the form factor but not precisely the right anomalous dimension. Hence, as anticipated earlier [37] (and expressing a result that can be understood via the behavior of the dressed-quark mass-function [5; 6]), one should expect dominance of hard contributions to the pion form factor for $Q^2 \gtrsim 8 \text{ GeV}^2$. Notwithstanding this, the normalization of the form factor is fixed by a pion wave-function whose dilation with respect to $\varphi_\pi^{\text{asy}}(x)$ is a definitive signature of dynamical chiral symmetry breaking.

Acknowledgements I wish to acknowledge valuable interactions with C. D. Roberts and Lei Chang that made a lot of this work possible. I also wish to thank the organizers of the LightCone 2013 workshop for

² A continuous scale evolution of $\varphi_\pi(x; Q)$ is ignored in Fig. 4 because it is too slow to be depicted properly on this limited Q^2 domain

providing a fine program and a welcoming atmosphere. This work was supported in part by the National Science Foundation under Grant No. NSF-PHY-1206187.

References

1. Chang, L., Roberts, C.D.: Tracing masses of ground-state light-quark mesons. *Phys.Rev.* **C85**, 052201 (2012)
2. Chen, C., Chang, L., Roberts, C.D., Wan, S., Wilson, D.J.: Spectrum of hadrons with strangeness. *Few Body Syst.* **53**, 293–326 (2012)
3. Wilson, D., Cloet, I., Chang, L., Roberts, C.: Nucleon and Roper electromagnetic elastic and transition form factors. *Phys.Rev.* **C85**, 025205 (2012)
4. Maris, P., Roberts, C.D., Tandy, P.C.: Pion mass and decay constant. *Phys. Lett.* **B420**, 267–273 (1998)
5. Chang, L., Roberts, C.D., Tandy, P.C.: Selected highlights from the study of mesons. *Chin.J.Phys.* **49**, 955–1004 (2011)
6. Bashir, A., Chang, L., Cloet, I.C., El-Bennich, B., Liu, Y.X., et al: Collective perspective on advances in Dyson-Schwinger Equation QCD. *Commun.Theor.Phys.* **58**, 79–134 (2012)
7. Cloet, I.C., Roberts, C.D.: Explanation and Prediction of Observables using Continuum Strong QCD. *Prog. Part. Nucl. Phys.* **77**, 1–69 (2014)
8. Chang, L., Cloet, I., Cobos-Martinez, J., Roberts, C., Schmidt, S., Tandy, P.: Imaging dynamical chiral symmetry breaking: pion wave function on the light front. *Phys.Rev.Lett.* **110**, 132001 (2013)
9. Maris, P., Roberts, C.D.: π and K meson Bethe-Salpeter amplitudes. *Phys. Rev.* **C56**, 3369–3383 (1997)
10. Chang, L., Roberts, C.D.: Sketching the Bethe-Salpeter kernel. *Phys. Rev. Lett.* **103**, 081601 (2009)
11. Cloet, I., Chang, L., Roberts, C., Schmidt, S., Tandy, P.: Pion distribution amplitude from lattice-QCD. *Phys.Rev.Lett.* **111**, 092001 (2013)
12. Braun, V., Gockeler, M., Horsley, R., Perlt, H., Pleiter, D., et al: Moments of pseudoscalar meson distribution amplitudes from the lattice. *Phys.Rev.* **D74**, 074501 (2006)
13. Qin, S.x., Chang, L., Liu, Y.x., Roberts, C.D., Wilson, D.J.: Interaction model for the gap equation. *Phys.Rev.* **C84**, 042202 (2011)
14. Chang, L., Roberts, C.D., Schmidt, S.M.: Dressed-quarks and the nucleon’s axial charge. *Phys.Rev.* **C87**, 015203 (2013)
15. Chang, L., Liu, Y.X., Roberts, C.D.: Dressed-quark anomalous magnetic moments. *Phys.Rev.Lett.* **106**, 072001 (2011)
16. Nakanishi, N.: Partial-Wave Bethe-Salpeter Equation. *Phys.Rev.* **130**, 1230–1235 (1963)
17. Nakanishi, N.: A General survey of the theory of the Bethe-Salpeter equation. *Prog.Theor.Phys.Suppl.* **43**, 1–81 (1969)
18. Nakanishi, N.: *Graph Theory and Feynman Integrals*, New York, USA: Gordon and Breach. (1971)
19. Bhagwat, M.S., Pichowsky, M.A., Tandy, P.C.: Confinement phenomenology in the Bethe-Salpeter equation. *Phys. Rev.* **D67**, 054019 (2003)
20. Brodsky, S.J., Roberts, C.D., Shrock, R., Tandy, P.C.: New perspectives on the quark condensate. *Phys. Rev.* **C82**, 022201 (2010)
21. Chang, L., Roberts, C.D., Tandy, P.C.: Expanding the concept of in-hadron condensates. *Phys.Rev.* **C85**, 012201 (2012)
22. Brodsky, S.J., Roberts, C.D., Shrock, R., Tandy, P.C.: Confinement contains condensates. *Phys.Rev.* **C85**, 065202 (2012)
23. Efremov, A., Radyushkin, A.: Factorization and Asymptotical Behavior of Pion Form-Factor in QCD. *Phys.Lett.* **B94**, 245–250 (1980)
24. Lepage, G.P., Brodsky, S.J.: Exclusive processes in perturbative quantum chromodynamics. *Phys. Rev.* **D22**, 2157 (1980)
25. Brodsky, S.J., Frishman, Y., Lepage, G.P., Sachrajda, C.T.: Hadronic Wave Functions at Short Distances and the Operator Product Expansion. *Phys.Lett.* **B91**, 239 (1980)
26. Braun, V., Korchemsky, G., Mueller, D.: The Uses of conformal symmetry in QCD. *Prog.Part.Nucl.Phys.* **51**, 311–398 (2003)
27. Mikhailov, S., Pimikov, A., Stefanis, N.: Theoretical description and measurement of the pion-photon transition form factor. *Few Body Syst.* **55**, 367–372 (2012)
28. Chang, L., Cloet, I., Roberts, C., Schmidt, S., Tandy, P.: Pion electromagnetic form factor at spacelike momenta. *Phys. Rev. Lett.* **111**, 141802 (2013)
29. Maris, P., Tandy, P.C.: The π , K^+ , and K^0 electromagnetic form factors. *Phys. Rev.* **C62**, 055204 (2000)
30. Huber, G., et al: Charged pion form-factor between $Q^2 = 0.60 \text{ GeV}^2$ and 2.45-GeV^2 . II. Determination of, and results for, the pion form-factor. *Phys.Rev.* **C78**, 045203 (2008)
31. Huber, G., Gaskell, D.: Jefferson lab experiment report No. E12-06-10. (2006)
32. Amendolia, S., et al: A Measurement of the Space-Like Pion Electromagnetic Form-Factor. *Nucl.Phys.* **B277**, 168 (1986)
33. Farrar, G.R., Jackson, D.R.: The pion form-factor. *Phys. Rev. Lett.* **43**, 246 (1979)
34. Horn, T., et al: Determination of the Charged Pion Form Factor at $Q^2 = 1.60$ and $2.45 \text{ GeV}/c^2$. *Phys.Rev.Lett.* **97**, 192001 (2006)
35. Alkofer, R., Bender, A., Roberts, C.D.: Pion loop contribution to the electromagnetic pion charge radius. *Int.J.Mod.Phys.* **A10**, 3319–3342 (1995)

-
36. Maris, P., Tandy, P.C.: The quark photon vertex and the pion charge radius. *Phys. Rev.* **C61**, 045202 (2000)
 37. Maris, P., Roberts, C.D.: Pseudovector components of the pion, $\pi^0 - \gamma - \gamma$ transition, and $F_\pi(Q^2)$. *Phys.Rev.* **C58**, 3659–3665 (1998)
 38. Holt, R., Gilman, R.: Transition between nuclear and quark-gluon descriptions of hadrons and light nuclei. *Rept.Prog.Phys.* **75**, 086301 (2012)
 39. Dudek, J., Ent, R., Essig, R., Kumar, K., Meyer, C., et al: Physics Opportunities with the 12 GeV Upgrade at Jefferson Lab. *Eur.Phys.J.* **A48**, 187 (2012)
 40. Roberts, H., Roberts, C., Bashir, A., Gutierrez-Guerrero, L., Tandy, P.: Abelian anomaly and neutral pion production. *Phys.Rev.* **C82**, 065202 (2010)
 41. Brodsky, S.J., Cao, F.G., de Teramond, G.F.: Evolved QCD predictions for the meson-photon transition form factors. *Phys.Rev.* **D84**, 033001 (2011)
 42. Bakulev, A., Mikhailov, S., Pimikov, A., Stefanis, N.: Comparing antithetic trends of data for the pion-photon transition form factor. *Phys.Rev.* **D86**, 031501 (2012)
 43. Eichmann, G.: Baryon form factors from Dyson-Schwinger equations. *PoS QCD-TNT-II*, 017 (2011)